Report

INTENSITY EFFECTS IN THE FORMATION OF STABLE ISLANDS IN PHASE SPACE DURING THE MULTI-TURN EXTRACTION PROCESS AT THE CERN PS

S. Machida, C.R. Prior, STFC Rutherford Appleton Laboratory, Didcot, UK
S. Gilardoni, M. Giovannozzi, S. Hirlander[1], A. Huschauer[1],
CERN, Geneva, Switzerland [1]also at Vienna University of Technology, Vienna, Austria

Abstract

The CERN PS utilises a Multi-Turn Extraction (MTE) scheme to stretch the beam pulse length to optimise the filling process of the SPS. MTE is a novel technique to split a beam in transverse phase space into nonlinear stable islands. The recent experimental results indicate that the positions of the islands depend on the total beam intensity. Particle simulations have been performed to understand the detailed mechanism of the intensity dependence. The analysis carried out so far suggests space charge effects through image charges and image currents on the vacuum chamber and the magnets iron cores dominate the observed behaviour. In this talk, the latest analysis with realistic modelling of the beam environment is discussed and it is shown how this further improves the understanding of intensity effects in MTE.

Presented at:
HB2016 Workshop

Geneva, Switzerland
July, 2016

INTENSITY EFFECTS IN THE FORMATION OF STABLE ISLANDS IN PHASE SPACE DURING THE MULTI-TURN EXTRACTION PROCESS AT THE CERN PS

S. Machida[*], C.R. Prior, STFC Rutherford Appleton Laboratory, Didcot, UK
S. Gilardoni, M. Giovannozzi, S. Hirlander[1], A. Huschauer[1], CERN, Geneva, Switzerland
[1]also at Vienna University of Technology, Vienna, Austria

Abstract

The CERN PS utilises a Multi-Turn Extraction (MTE) scheme to stretch the beam pulse length to optimise the filling process of the SPS. MTE is a novel technique to split a beam in transverse phase space into nonlinear stable islands. The recent experimental results indicate that the positions of the islands depend on the total beam intensity. Particle simulations have been performed to understand the detailed mechanism of the intensity dependence. The analysis carried out so far suggests space charge effects through image charges and image currents on the vacuum chamber and the magnets iron cores dominate the observed behaviour. In this talk, the latest analysis with realistic modelling of the beam environment is discussed and it is shown how this further improves the understanding of intensity effects in MTE.

INTRODUCTION

The Multi-Turn Extraction (MTE) scheme at cERN was conceived as method of beam transfer from the PS to the SPS to minimise beam loss [1]. It has been demonstrated experimentally several times [2] and is now in daily operation. It has also been suggested that an inverse process could be utilised for Multi-Turn Injection (MTI).

The mechanism of beam splitting and preservation of the separated beamlets can be identified as a nonlinear resonant driving term (octupole in this study) and amplitude dependent tune shift. In other words, the essential ingredients are the non-zero harmonic component of the multipole potential and zero-th component of the multipole potential (this can be the same multipole as the other). It is, however, not clear how the beam intensity affects the dynamics.

Experimental observation shows that the beamlets move outward as the beam intensity increases [3]. We have included a simple model of space charge effects in the MTE simulation that starts after the process of beam splitting to see how the beam intensity changes the beamlets' position in the phase space.

MODEL

Generally speaking, when space charge effects are included in particle tracking simulation, the charge distribution of each beamlet as well as its position in the transverse phase space should be updated self-consistently. The distributions are no longer determined only by the lattice elements. On the other hand, the beamlets are reasonably separated in the

configuration space. Therefore we assume that only the position of each beamlet is modified by the interaction between the charge centres of the beamlets and is insensitive to the details of the charge distribution. This justifies the introduction of a frozen space charge model. The charge distribution is fixed at the start of the simulation and not updated after each integration step. However, one significant difference from the ordinary frozen model for a single beam is that the beamlet positions are calculated iteratively. When there is only a single beam, it always sits at the centre of phase space, which may be slightly shifted by closed orbit distortion. When there are multiple beamlets, contributions to the space charge potential from other beamlets produce dipole kicks which we take into account to solve for the beamlet positions self-consistently.
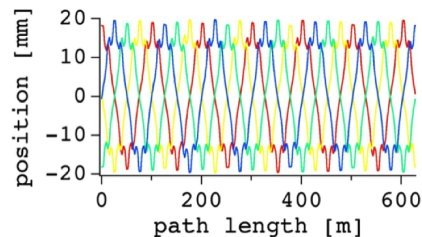

Figure 1: Position of the stable fixed points around the ring. They are all connected to make a closed orbit returning to the initial point after 4 turns.

In practice, to include space charge effects among the beamlets, the position of stable fixed points without space charge is first calculated everywhere in the ring, along an orbit that returns to the initial phase space point after 4 turns. This closed orbit is in addition to the normal orbit around the centre which comes back to the initial point on every turn. The position around the ring is shown in Fig. 1. Different colours indicate the evolution of each fixed point, but they are all connected making one single closed orbit. Once the fixed point positions are identified, space charge effects can be included by centring the space charge potential at that position. With a small time step, typically 10 ns, a particle is tracked taking into account the external magnetic lattice as well as the space charge potential.

Obviously, the closed orbit coming back after 4 turns under space charge is different from the orbit without space charge. That means that the position of the beamlets has to be adjusted to the new position and then the closed orbit has to be calculated again. This iteration repeats until the closed orbit found by the particle tracking agrees with the position

of the beamlets identified before the tracking. About 10 iterations are enough to obtain adequate convergence provided such a closed orbit exists. In some cases, for example with extremely strong space charge, there is no fixed point and no convergence after many iterations.

So far only direct space charge potential has been considered. There are also image charges (electric) and image currents (magnetic) on the vacuum chamber and magnet pole faces, respectively. As we assume horizontal parallel plates for both the electric and magnetic boundary, there is an infinite number of image charges and current layers. In simulation, a sufficient number of layers of the image charges and currents is determined by looking at the convergence of the fixed point position as a function of the layers. The deviation of the fixed point position is within 1% when more than 10 layers (for image changes and image currents separately) are included.

In the case of parallel boundary conditions, we can construct an analytical model on the direct as well as image charge and image current contributions. For purposes of illustration, we first discuss the model with one beamlet at the centre and two beamlets at a distance from the centre. The outer two beamlets oscillate around the central beamlets in phase space. This model is not expected to lose the generality of the full multi beamlets situation as far as space charge interaction is concerned.

Let us first consider the contributions from the direct space charge and current for completeness. A repulsive electric force between particles with charges of the same sign weakens the restoring force so the betatron tune shift is negative. This is true for particles in the outer beamlets as well. As in a single beam, moving charges create a magnetic field that produces a force in the opposite direction to the electric repulsive force with a factor of $-\beta^2$, where β is the speed of particles normalised with the speed of light c. We consider only the horizontal direction.

$$F_{\text{direct, elec+magn}} = (1 - \beta^2)\frac{3e\lambda}{4\pi\varepsilon_0}\frac{1}{x},$$

where e is the electric charge, λ is the line density, ε_0 is the permittivity of free space. The sum of electric and magnetic forces with a factor of $(1-\beta^2)$ is still repulsive, but it becomes less when the beam momentum is high, e.g. at the extraction energy.

When there is a metallic boundary made up of parallel plates with half height h, image charges appear on the other side of the plates. Individual particles feel an attractive force, which strengthens the restoring force in the horizontal direction and weakens the restoring force in the vertical direction.

$$F_{\text{image, elec, s1}} = -\frac{e\lambda}{\pi\varepsilon_0}\frac{x}{(2h)^2 + x^2}.$$

We can extend this model to the multiple beamlets case. Having the image charge of other beamlets on the other side of vacuum chamber plates, the restoring force of the
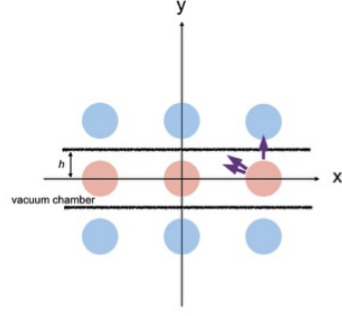

Figure 2: In addition to the force between the beamlet on the mid plane and its image, there is another force between the beamlet and the image charge of other beamlets indicated as two arrows pointing left. There should be force between the beamlets and the images below the vacuum chamber plate as well. As a result, restoring force to the outer beamlets with respect to the centre increases.

outer beamlets with respect to the oscillation centre becomes stronger as you can see in Fig. 2.

$$F_{\text{image, elec, m1}} = -\frac{e\lambda}{\pi\varepsilon_0}\left[\frac{x}{(2h)^2 + x^2} + \frac{2x}{(2h)^2 + (2x)^2}\right].$$

Of course, there is infinite layer of image charges with alternating signs. The image charge in the second layer acts to cancel the force of the first one, but not completely because the distance of the interaction is greater.

$$F_{\text{image, elec, ms}} = -\frac{e\lambda}{\pi\varepsilon_0}\Big[\frac{x}{(2h)^2 + x^2} + \frac{2x}{(2h)^2 + (2x)^2} \\ - \frac{x}{(4h)^2 + x^2} - \frac{2x}{(4h)^2 + (2x)^2} + \cdots\Big].$$

Notice that there is no image current at the same place of the image charge. Although the orbit of the beamlets oscillates around the ring, it does not move in time. Only a DC component of magnetic field is created, which can penetrate the metallic vacuum chamber wall. On the other hand, the DC component of the magnetic fields makes an image current on the magnet pole face. Let us assume the half gap of the magnet pole face is g.

$$F_{\text{image, magn, ms}} = \beta^2\frac{e\lambda}{\pi\varepsilon_0}\Big[\frac{x}{(2g)^2 + x^2} + \frac{2x}{(2g)^2 + (2x)^2} \\ - \frac{x}{(4g)^2 + x^2} - \frac{2x}{(4g)^2 + (2x)^2} + \cdots\Big].$$

This simple analytical model helps us understand how the direct and image space charge forces act, at least whether the overall effect is repulsive or attractive.

RESULTS

Two octupoles in the straight sections 39 and 55 (IOCT39 and IOCT55) and two sextupoles next to the octupoles in the same straight sections IXCT39 and IXCT55 are excited.

The pole face winding has a set current close to the machine operation condition. The magnet packing factor, defined as the fraction of the total magnet length over the circumference, is 0.8. The tunes without space charge are (6.255, 6.230).
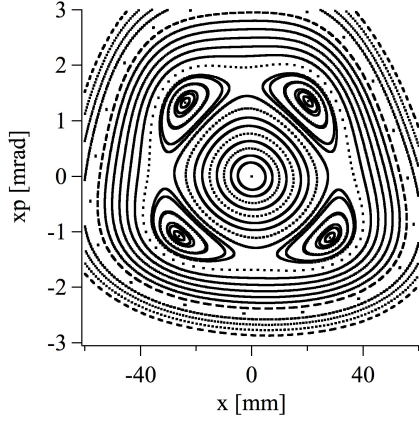

Figure 3: Horizontal phase space with islands when no space charge potential is included.
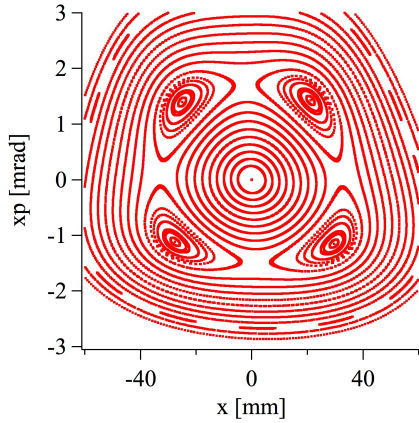

Figure 4: Phase space when the space charge from a total beam intensity of 3.27×10^{13} is included. The beam intensity of each beamlet is equal, namely 1/5 of the total beam intensity.

Figures 3 and 4 show the horizontal phase space without and with space charge effects from a total 3.27×10^{13} protons (shared equally across 5 beamlets). Figure 5 is the close-up view of the lower right island.

Figure 6 shows the intensity dependence of the fixed point locations with different boundary conditions. When only direct space charge is included, the islands move inwards (blue), but the change is small at the high beam momentum of 14 GeV/c. Image charges induce a large shift outwards (green). Image currents cause inward displacement that tends to cancel the image charge contributions.

In the simulation above, we assumed that all the five beamlets including at the centre have equal intensity. In order to see how an imbalance in beam intensity changes the behaviour, an *intensity imbalance factor* f is introduced be-
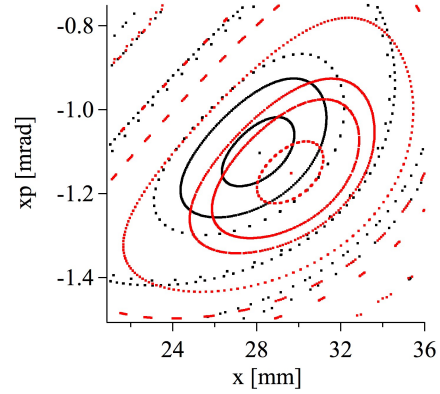

Figure 5: Close view of the lower right island. Black dots show the zero intensity case of Fig. 3 and red dots show the effect of space charge from Fig. 4. Single dots of black and red around the centre of each coloured ellipse indicate the fixed points.
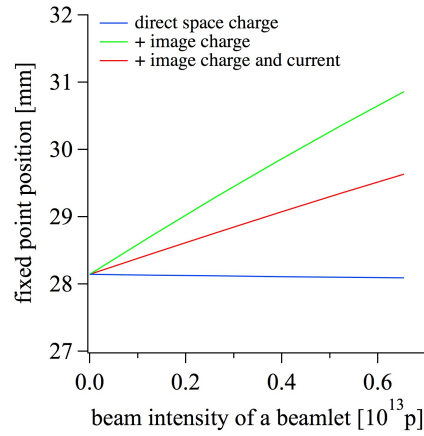

Figure 6: Location of the lower right island in Fig. 4 *v.* total beam intensity. Direct space charge produces a slightly negative tune shift and the island moves inwards with intensity. Image charge only gives a positive tune shift and the island moves outwards. Image current partially cancels the tune shift, and the slope of the line is less than the case with image charge only. The beam momentum is 14 GeV/c, the vacuum chamber half-height is h=35 mm, and the magnet pole face half-height is g=50 mm. We assume parallel plates to model the vacuum chamber and magnet pole faces. The packing factor of the magnets is 0.8. The total beam intensity is five times the beamlet intensity.

tween the core and the outer beamlets as follows,

$$I_{\text{core}} = (1 + 4f) \times I_{\text{eq}},$$
$$I_{\text{outer}} = (1 - f) \times I_{\text{eq}}$$

where I_{core} is the intensity in the core beamlet and I_{outer} is the intensity in each outer beamlet. When f is zero, all five beamlets have equal intensity I_{eq}. When $f = -0.25$, there is no beam in the centre and the whole intensity is shared by the outer beamlets equally. When $f = 1.0$, there are no

outer beamlets and only the central beamlet exists. The total beam intensity is kept constant.
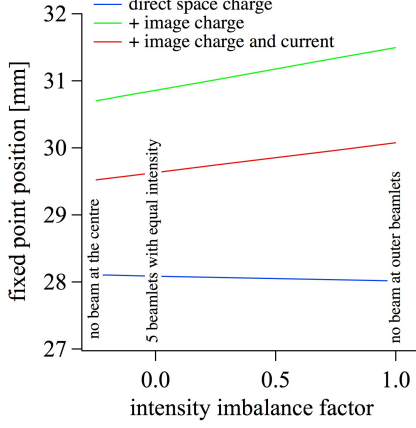

Figure 7: Fixed point position as a function of the intensity imbalance factor (see text).

Figure 7 shows how the fixed points move as a function of the intensity imbalance factor. The total beam intensity is fixed at 3.27×10^{13} and the horizontal tune used is the nominal tune, 6.255. The fixed point at zero current is positioned at 28.143 mm. The shift due to an imbalance in the beam intensity is rather small.
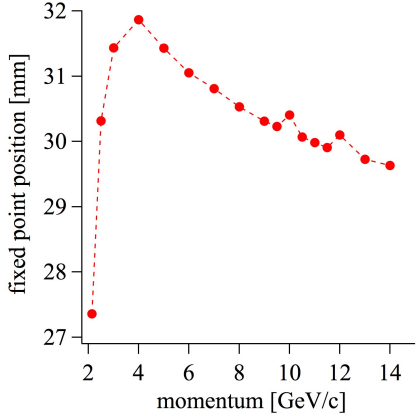

Figure 8: Fixed point position as a function of beam momentum.

Finally, the position of the fixed points as a function of beam momentum is shown in Fig. 8. Although there are some fine structures at momenta around 10 and 12 GeV/c whose reason is unknown, at the lower momentum, direct space charge effects are dominant. As the beam momentum increases, the contribution from the image charge/current becomes large and overcomes the direct space charge. As the beam momentum becomes even higher, the image charge/current space charge effects decrease due to the relativistic Lorentz factor.

COMPARISON WITH EXPERIMENT

So far, we have used parallel plates models for both the electric boundary image charges and the magnetic boundary image currents. However, more realistic boundary conditions have to be implemented in order to compare results from the simulation and experiment quantitatively. As a first step, a rectangular boundary has been introduced to treat the electric boundary.

We use the model in [4]. here Poisson's equation is solved by invoking a conformal Schwarz-Christoffel transformation.

$$G(u, v, u_0, v_0) = \frac{1}{4\pi} \ln \frac{(u - u_0)^2 + (v + v_0)^2}{(u - u_0)^2 + (v - v_0)^2},$$

where $G(u, v, u_0, v_0)$ is a Green's function and (u, v) and (u_0, v_0) are the transformed coordinates of the observation and source points, respectively. The mapping relations between coordinates before transformation (x, y) and after (u, v) are,

$$u = \frac{\operatorname{sn}(2Kx/a, k) \operatorname{dn}(2Ky/a, k')}{1 - \operatorname{dn}^2(2Kx/a, k) \operatorname{sn}^2(2Ky/a, k')},$$
$$v = \operatorname{cn}(2Kx/a, k) \operatorname{dn}(2Kx/a, k)$$
$$\times \frac{\operatorname{sn}(2Ky/a, k') \operatorname{cn}(2Ky/a, k')}{1 - \operatorname{dn}^2(2Kx/a, k) \operatorname{sn}^2(2Ky/a, k')},$$

where K is the complete elliptic integral of the first kind with module k and residual module k'. sn, cn and dn are the Jacobi elliptic functions. a and b are the horizontal and vertical aperture, respectively.

The electric field is the derivative of the potential. In order to calculate electric fields numerically, a circular cross-section beam of 2 mm radius with a uniform charge distribution is assumed. With this assumption, the electric fields at the beam edge are calculated numerically as

$$E_x = -\frac{G(x + dx, y, x_0, y_0) - G(x - dx, y, x_0, y_0)}{2dx},$$
$$E_y = -\frac{G(x, y + dy, x_0, y_0) - G(x, y - dy, x_0, y_0)}{2dy},$$

where dx and dy are set to 0.1 mm. Electric fields inside the beam are a linear function of the coordinates (x, y) and zero at the centre.

Ignoring image currents on the magnet pole face for the moment, the force acting on the beam particles in the rest frame has two components,

$$F_{\text{total}} = \left(1 - \beta^2\right) F_{\text{direct, elec}} + F_{\text{image, elec}}.$$

The field obtained with the boundary conditions is the sum of the direct electric field and the image charge electric field. In order to calculate the direct magnetic field, we need the direct electric field without boundary. This has been done by assuming a vacuum chamber 100 times larger (the results are almost the same with 10 times larger). Finally, the force

is the combination of the following terms,

$$F_{\text{total}} = \left(1 - \beta^2\right) F_{\text{direct, elec}} + F_{\text{direct+image, elec}}$$
$$- F_{\text{direct, elec}} .$$

The second term on the right hand side is the field obtained by solving for the potential with rectangular boundary conditions.
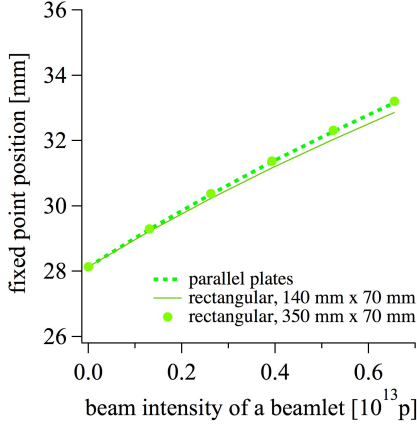

Figure 9: Fixed point position as a function of horizontal tune. The bare tunes are (6.255, 6.300). There is a slight difference between the results from parallel plates and a rectangular vacuum chamber.

We have compared the fixed point position as a function of beamlet intensity with different boundary conditions. Figure 9 shows that the parallel plates model and the rectangular vacuum chamber model give a slightly different intensity dependence. In order to check the consistency of two models, the results for a wider rectangular aperture are also shown in each case as solid circles. It is confirmed that the rectangular vacuum chamber gives similar results to those from parallel plates.

In reference [3] Fig. 13 and TAble IV, the beamlet position as a function of the total beam intensity is shown and tabulated. These can now be compared with the corresponding simulation results. Figure 10 shows the slope of each beamlet. There are two simulation results: the first includes everything: direct space charge, image charges on the vacuum chamber and image currents on magnets; the second excludes image currents on magnets. Overall, experimental and simulation results look similar but there are two obvious discrepancies. First, the simulation results are equally distributed below and above zero whereas three experimental results have a positive slope and one has a negative slope. Secondly the difference between the maximum and the minimum slopes seems slightly different between simulation and experiment. We are investigating sources of the discrepancies.

One of the experimental findings - that there is no difference between debunched and bunched beams in terms of intensity dependence of beamlet position - can be understood if the main space charge contribution is from image charges and image currents. Each depends only on the total intensity and not on the bunching factor. This excludes the dependence of a longitudinal model in the simulation.

REFERENCES

[1] R. Cappi and M. Giovannozzi, Phys. Rev. Lett. **88**, 104801 (2002).

[2] S. Gilardoni, M. Giovannozzi, M. Martini, E. Metral, P. Scaramuzzi, R. Steerenberg and A.-S. Muller, Phys. Rev. ST Accel. and Beams **9**, 104001 (2006).

[3] Simone Gilardoni, Massimo Giovannozzi and Cedric Hernalsteens, Phys. Rev. ST Accel. and Beams **16**, 051001 (2013).

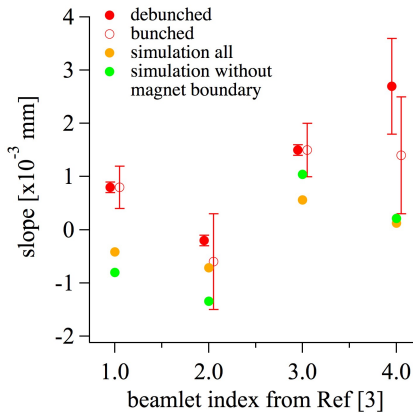[4] Q. Shou, Q Jiang and Q Guo, J. Phys. A: Math. Theor. **42** (2009) 205202.

Figure 10: Slope of the beamlet position as a function of total beam intensity observed experimentally and by simulation. the slope is defined as a function of the total beam intensity of 10^{10} as in [3].